Materials Research Bulletin 61 (2015) 551–559

Contents lists available at ScienceDirect

Materials Research Bulletin

journal homepage: www.elsevier.com/locate/matresbu

Thermoelectric, electronic, optical and chemical bonding properties of Ba_2PrRuO_6: At temperature 7 K and 150 K

A.H. Reshak [a,b], Wilayat Khan [a,*]

[a] New Technologies-Research Center, University of West Bohemia, Univerzitni 8, 306 14 Pilsen, Czech Republic
[b] Center of Excellence Geopolymer and Green Technology, School of Material Engineering, University Malaysia Perlis, Kangar, Perlis 01007 Malaysia

ARTICLE INFO

Article history:
Received 29 September 2013
Received in revised form 22 March 2014
Accepted 5 October 2014
Available online xxx

Keywords:
FPLAPW calculations
Electronic structure
Fermi surface
Charge density
Optical properties
Thermoelectric properties

ABSTRACT

We present first principles calculations of the band structure, density of states, electronic charge density, Fermi surface and optical properties of Ba_2PrRuO_6 single crystals at two different temperatures. The atomic positions were optimized by minimizing the forces acting on the atoms. We have employed the full potential linear augmented plane wave method within local density approximation, generalized gradient approximation and Engel–Vosko generalized gradient approximation to treat the exchange correlation potential. The calculation shows that the compound is superconductor with strong hybridization near the Fermi energy level. Fermi surface is composed of two sheets. The calculated electronic specific heat capacities indicate, very close agreement with the experimental one. The bonding features of the compounds are analyzed using the electronic charge density in the (1 0 0) and (0–10) crystallographic planes. The dispersion of the optical constants was calculated and discussed. The thermoelectric properties are also calculated using the BoltzTrap code.

1. Introduction

The composition of the double ordered perovskites $A_2BB'O_6$ are possibly be the most studied family of compounds because of their intrinsic ability to provide a spacious range of elemental compositions and they exhibit a wealth of structure variations. Up till now, it is found that most of the alloys have rock salt configuration, by changing the perovskite units ABO_3 and $AB'O_3$ along the three crystalline directions. Recently, among these perovskites, the mixed-metal oxides contains ruthenium were prepared make use of molten hydroxide fluxes, their structures and magnetic susceptibility were investigated [1–5]. Perovskite-type materials show broader range of physical properties, due to which these compounds are of great interest to material science [6]. These materials exhibit high ionic and electronic conductivity displayed by oxygen lacking perovskites [7–9]. High ionic conductivity generally takes the pattern of either high oxygen anion conductivity, as originate in $La_{1-x}Sr_xGaO_{3-\delta}$ [10] or proton conductivity, for instance in $BaCeO_{3-\delta}$ [11] or $Ba_2YSnO_{5.5}$ [12]. Perovskites with such properties are useful for relevance in solid oxide fuel cells, high-temperature oxygen parting, electrochemical reactors and oxygen sensors [6,13].

Recently, the researchers have started to investigate the conductivity and magnetic properties of oxides based on Ru [14–20], after the discovery of superconductivity in Sr_2RuO_4 [21]. The term double perovskite is commonly used to explain B-site ordered perovskites of the general formula $A_2BB'O_6$. Many research groups start examining the large family of double perovskites containing Ba_2PrRuO_6 [22–28]. The polycrystalline samples of BaPr2116 synthesized at high temperature sintering of stoichiometric powder and studied by Izumiyama et al. [29].

The fascinating magnetic properties arise from the regular arrangement of the cations within this structure. A_2LnMO_6 (A = alkaline earth elements; Ln = rare earth elements; M = 4d or 5d transition elements) are ordered double perovskite-type oxides, in which both the Ln and M are regularly ordered elements and give rise different types magnetic characteristics at low temperature. Sometimes, the highly oxidized cations like Ru^{+5} ions electronic structure is [Kr] $4d^3$ ([Kr]: krypton core) from the second transition series exhibit complicated magnetic behavior. Wu and co-workers [14,30,31] examined $Ba_2YRu_{1-x}Cu_xO_6$ (BaYCu2116) and $Sr_2YRu_{1-x}CuxO_6$ (SrYCu2116), polycrystalline samples belong to the family of double perovskites, and stated the occurrence of superconductivity and magnetism for $x = 0.05$ to 0.2. The electronic and structural properties of R_2NiMnO_6 (R = Pr,

* Corresponding author. Tel.: +42 775 526 684.
E-mail address: walayat76@gmail.com (W. Khan).

http://dx.doi.org/10.1016/j.materresbull.2014.10.028
0025-5408/

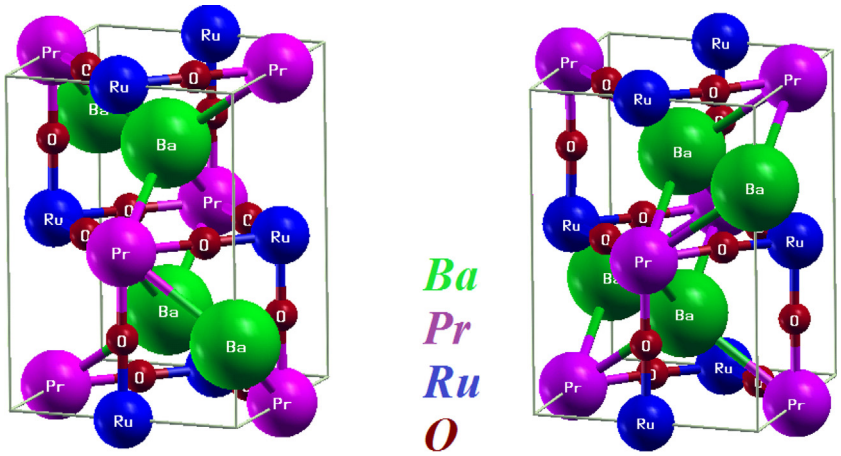

Fig. 1. Molecular structures of both compounds BPRO (150 K, 7 K).

Nd, Sm, Gd, Tb, Dy, Ho, and Y) have been studied by Lofland et al. [32].

From above we noticed that there is a lack information about the electronic, thermoelectric and optical properties of Ba_2PrRuO_6 single crystals which were experimentally prepared at different temperatures (7 K and 150 K) [33]. Thus, we have addressed ourselves to calculate the electronic and optical properties, using full potential method. Using BoltzTrap code we also have calculated the thermoelectric properties namely, Seebeck coefficient, electrical conductivity, thermal conductivity, and power factor versus temperature to get better information about the material efficiency.

2. Computational method

The under investigation compounds Ba_2PrRuO_6 (which were experimentally prepared at 7 K and 150 K [33]) has monoclinic structure with space group P21/n (#14), their optimized structures is shown in Fig. 1. Here in this paper, for simplicity we represent these compounds as BPRO (7 K) and BPRO (150 K) respectively. Calculations were performed using the experimental data taken from Ref. [33], as starting point for this work. The density functional theory (DFT) [34], namely the full potential linear augmented plane wave (PF-LAPW) method, as implemented in the WIEN2k code [35] was used. The exchange-correlation (XC) potential was treated within Ceperley–Alder local density approximation (LDA) [36], and Perdew–Burke–Ernzerhof generalized gradient approximation (PBE-GGA) [37]. In addition the Engel–Vosko generalized gradient scheme (EVGGA) [38] was used. It is well known that the EVGGA approach yield better result as compared to LDA and GGA. In FP-LAPW technique, the unit cell is divided in to non-overlapping atomic spheres (centered at the atomic sites) and the interstitial region. The value of the maximum angular quantum number(*l max)* for atomic wave function inside

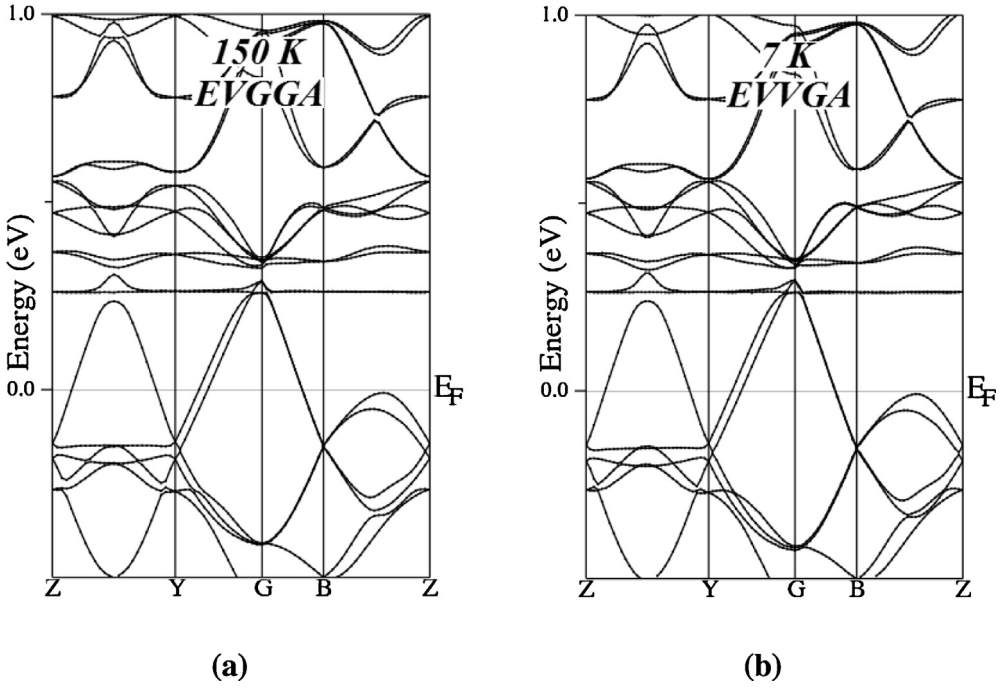

Fig. 2. Calculated band structures of both compounds BPRO (150 K, 7 K) using (a) EVGGA.

the spheres was 10. Self consistency was obtained by using the 96 k-points in the irreducible Brillouin zone (IBZ), using the Monkhorst pack special k-points approach [39]. The convergence in the energy eigenvalues is obtained, when the wave function in the interstitial region is expanded in plane waves with the cut-off $K_{max} = 7/R_{max}$, where K_{max} stands for the magnitude of the largest K vector expanded in plane wave and R_{max} stands for the smallest atomic sphere radii. The maximum Fourier expansion of change density cut-off $G_{max} = 13$ (a.u.)$^{-1}$ was used. The value of the muffin ten radii are 2.5, 2.20, 2.01, and 1.78 a.u for Ba, Pr, Ru, and O atoms, respectively of both compounds. These radii are taken in such a way that it protects the leakage of charges from their respective sphere.

3. Result and discussion

3.1. Electronic structure

The calculated electronic band structures of the investigated compounds along the high symmetry points of the Brillouin zone (BZ) are shown in Fig. 2a and b. Both compounds have quit similar band structures (Fig. 2b). To the best of our knowledge there is no experimental data for the band structure are available in the literature to make meaningful comparison. It is clear that the upper valence band is mainly formed by Pr-f and Ru-d states for BPRO compounds at 7 K and 150 K. The electronic band structure shows the superconducting nature of the compounds due to the considerable overlapping of valence and conduction bands at Fermi level.

In order to realize the bonding natures, Fig. 3(a–n), shows the total density of states (DOS) and partial density of states (PDOS) for BPRO (7 K and 150 K).

The general relation used to generate the DOS plots is [40]:

$$\mathrm{DOS}(\varepsilon) = \sum_{i=1}^{N} \left(\left[\frac{n_i}{\omega\left(\frac{\pi}{2}\right)^{1/2}} \times \exp\left(\frac{-2(\varepsilon - \varepsilon_i)^2}{\omega^2} \right) \right] + \left[\frac{2n_i\omega}{\pi\left(\omega^2 + 4(\varepsilon - \varepsilon_i)^2\right)} \right] \right)$$

Fig. 3a and b shows that EVGGA cause to shift all the structures of BPRO (7 K and 150 K) towards lower energies as compared to structures obtained by LDA and GGA. That is attributed to the fact that EVGGA produce better band splitting compared to LDA and GGA. Therefore we decided to show the PDOS which obtained by EVGGA. It is clear from Fig. 3 that the valence band is divided into four parts which are labeled as A–D. The lowest energy part (A) is positioned in the energy range (−18.0 eV to −15.0 eV) where the states Pr-p and O-s have strong contribution, and the states Ru-p, Pr-s, and Ru-s exhibit small contribution. The states Ba-p contributed strongly to the next part (B) and the remaining states have negligible contributions. The third lowest band (c) ranging from −10.0 eV to −5.0 eV which originates from the negligible contributions of all states of BPRO (7 K and 150 K) as displayed in Fig. 3. The last part of the valence band is located in the range between −5.0 eV and 0.0 eV is arise mainly from Ru-d and O-p states (double peaked structure), and the remaining states have negligible contribution. Following Fig. 3, a small shift is observed in Ru-s state of BPRO (7 K) as compared to Ru-s state of BPRO (150 K). It is obvious that when we compare BPRO (7 K) with BPRO (150 K), the amplitudes of DOS (states/eV unit cell), at the valence band is increased for each states of BPRO (150 K) with respect to BPRO (7 K). The transition metal series depict the most delocalized d-state (anti-bonding states), exhibit greater density of states. Due to the smallest interaction with the adjacent atoms, these states spread over small energy range [41].

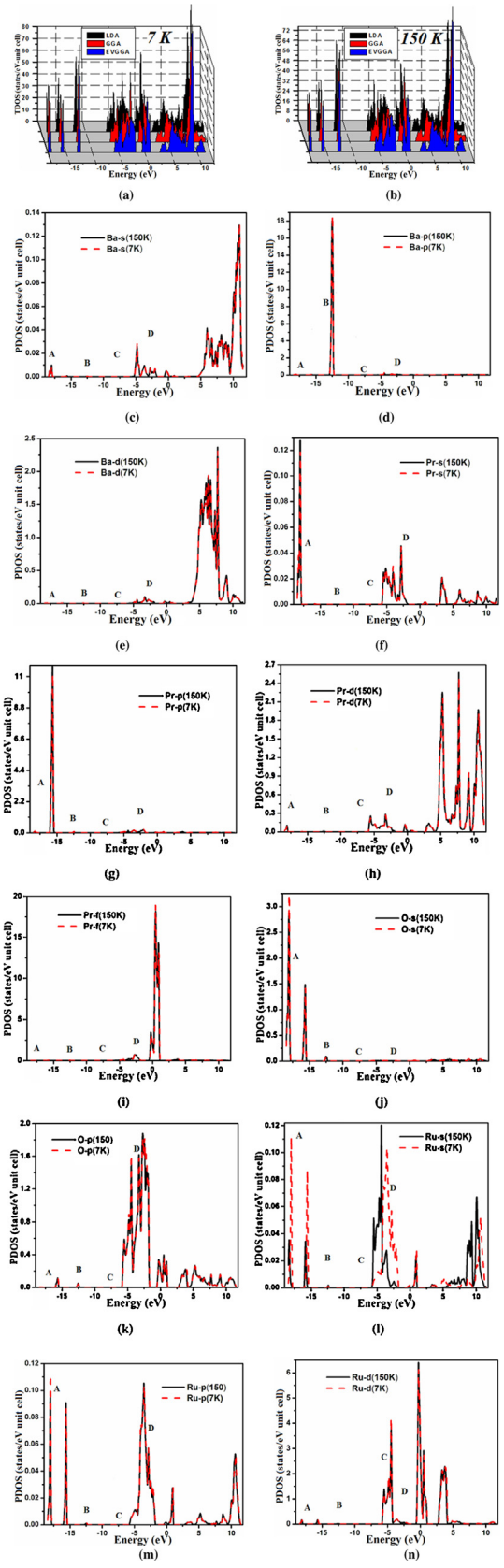

Fig. 3. Calculated total density state (DOS) and partial density of states (PDOS) of both compounds BPRO (150 K, 7 K).

We would like to mention that the large density of state at Fermi level N (E_F) confirm the superconducting behavior of BPRO (7 K and 150 K). The $N(E_F)$ values are 11.26 (LDA), 12.02 (GGA), and 17.6 (EVGGA) states/eV unit cell, for BPRO (150 K) and 11.5 (LDA), 12.6 (GGA) and 16.9 (EVGGA) states/eV for BPRO (150 K).

We have calculated the electronic specific heat capacity (γ) using the following relation:

$$\gamma = \frac{1}{3}\pi^2 N(E_F) K_\beta^2 \quad (1)$$

in the above relation $N(E_F)$ represent DOS at E_F and K_β represent the Boltzmann constant. The calculated values for the specific heat for BPRO (150 K) are 1.95 mJ/mol – k^2(EVGGA), 2.085 mJ/mol – k^2(GGA), and 3.05 mJ/mol – k^2(LDA), while for BPRO (7 K) are 1.99 mJ/mol – k^2 (EVGGA), 2.18 mJ/mol – k^2(GGA), and 2.93 mJ/mol – k^2(LDA). We should emphasize that the values of electronic specific heat capacity for BPRO (7 K and 150 K) using EVGGA show very good agreement with the experimental values of the specific heat capacity [42], which confirm the accuracy of our calculations.

3.2. Electronic charge density

Fig. 4a and b shows contour plots of electronic charge density in (1 0 0) and (0 1 0) crystallographic planes for BPRO compound at 7 K and 150 K. Following these figures one can see that the charge concentration around oxygen atom is greater than other atoms like barium, praseodymium and ruthenium, due to greater electronegativity of oxygen atom. It is clear that the electronic charge densities contours show homogeneous charge distribution, which display that O atom show covalent bond with nearest Pr atom due to the robust overlapping of Pr and O orbital, while O atom with Ru form polar covalent bond, due to weak overlapping Ru and O orbital. On the other hand Ba atom has ionic nature and small hump appear towards O atom due to high electronegativity, which led to attract the electrons of Ba atoms. It is also clear from Fig. 4a and b that the interacting atoms exhibit maximum electronic charge density as compared to the ionic ones, which need effective charge transfer. We illustrate from the thermo scale that blue color exhibit greater charge density. Therefore, the oxygen atoms have greater charge density than the other atoms.

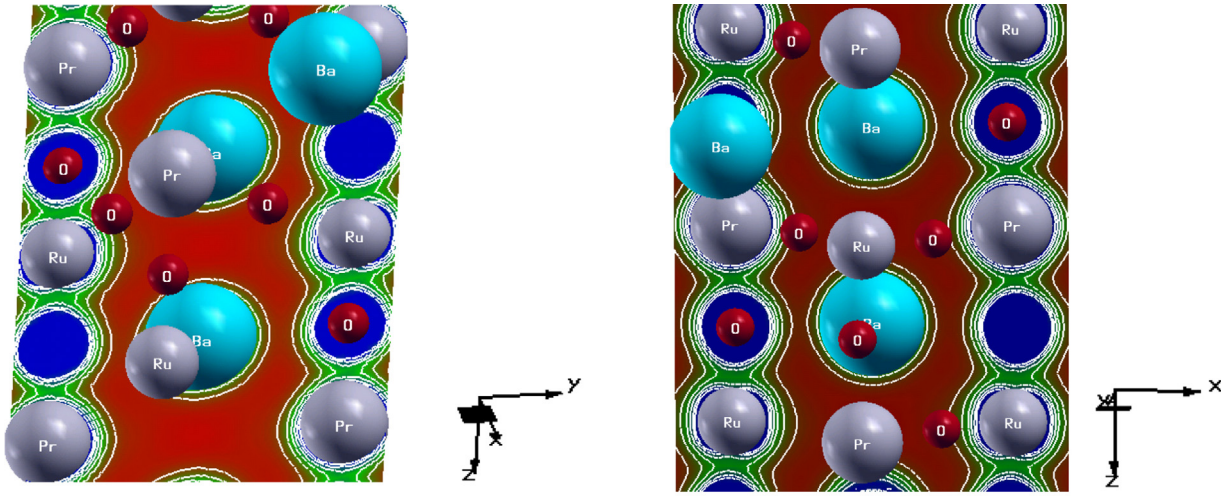

(a) for 150K (100) and (010)

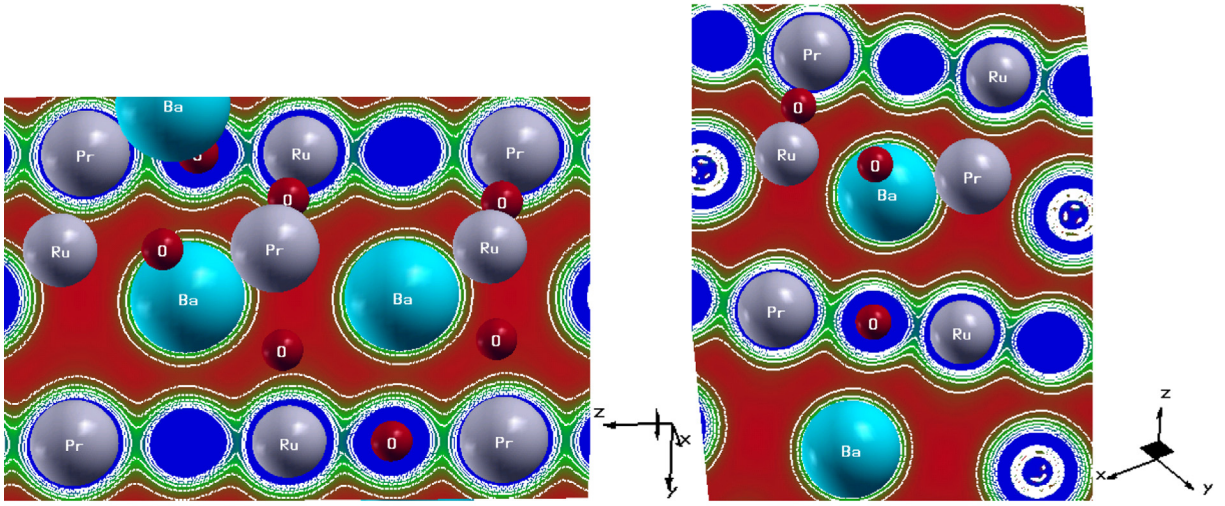

(b) for 7 K (100) and (010)

Fig. 4. Electronic charge density distribution contour calculated with mBJ in the (010) and (010) planes of both compounds BPRO (150 K, 7 K).

3.3. Fermi surface

The occupation of the bands around Fermi level describes the superconducting nature of the compounds. For this purpose, it is of great interest to plot the Fermi surface (FS). It plays a key role to explain the electronic structure of any superconducting material. We use FS to calculate the energy distribution curve (EDC) for typical k-points of the Brillioun zone and to determine the location of the k-points where the bands pass through Fermi level. The electrons around the Fermi level cause the electrical conductivity. From the experimental point of view, the de Haas van Alphen (dHvA) experiments used to investigate the Fermi surface; the exact measurement of the structure of the FS depends on models using simple geometries, which is able to specify both the magnetic field angle dependency of the calculated frequencies, but the exact structure of the FS can be of course much further complex. For this reason, we plot the FS for BPRO compound at 7 K and 150 K using FP-LAPW techniques as shown in Fig. 5(a and b). Following these figures we predict that there are two bands crossing the Fermi level along the $\Gamma - Z$ direction. The FS of BPRO compound at 7 K and 150 K contain both set of holes (the empty region) and electronic sheets (shaded region), and the empty region decreased by replacing BPRO (7 K) on BPRO (150 K). The change in electron velocity is examined from the color changes in the merge band of Fermi surface in fig., i.e., the red color show fast velocity and violet show small velocity, while the remaining color show intermediate velocity of the electrons [43,44]. One can also examine from merged bands of BPRO compound at 7 K and 150 K (Fig. 5) that the compound BPRO (150 K) exhibit good electrical conductivity, as compared to the BPRO (7 K), because the red color (fast velocity) is greater for BPRO compound at 7 K than that at 150 K. From our investigated Fermi surface, we get topology of the different electron system, which is closely related to the electron transport properties of the materials, such as electrical conductivity.

3.4. Optical properties

Since, the investigated compound have monoclinic symmetry with space group (No. $P2_1/c$), this symmetry allows several none zero components for the second order dielectric function along the crystallographic directions. We will focus only on $\varepsilon^{xx}(\omega)$,$\varepsilon^{yy}(\omega)$ and $\varepsilon^{zz}(\omega)$, which totally describe the dispersion of linear optical properties. The linear optical properties are obtained from complex dielectric-tensor given by the following equation:

$$\varepsilon(\omega) = \varepsilon_1(\omega) + i\varepsilon_2(\omega \tag{2}$$

where $\varepsilon_1(\omega)$ is the real part and $\varepsilon_2(\omega)$ is the imaginary part of the dielectric function. The frequency dependent imaginary part $\varepsilon_2(\omega)$ is obtained from the total density of states (TDOS) and

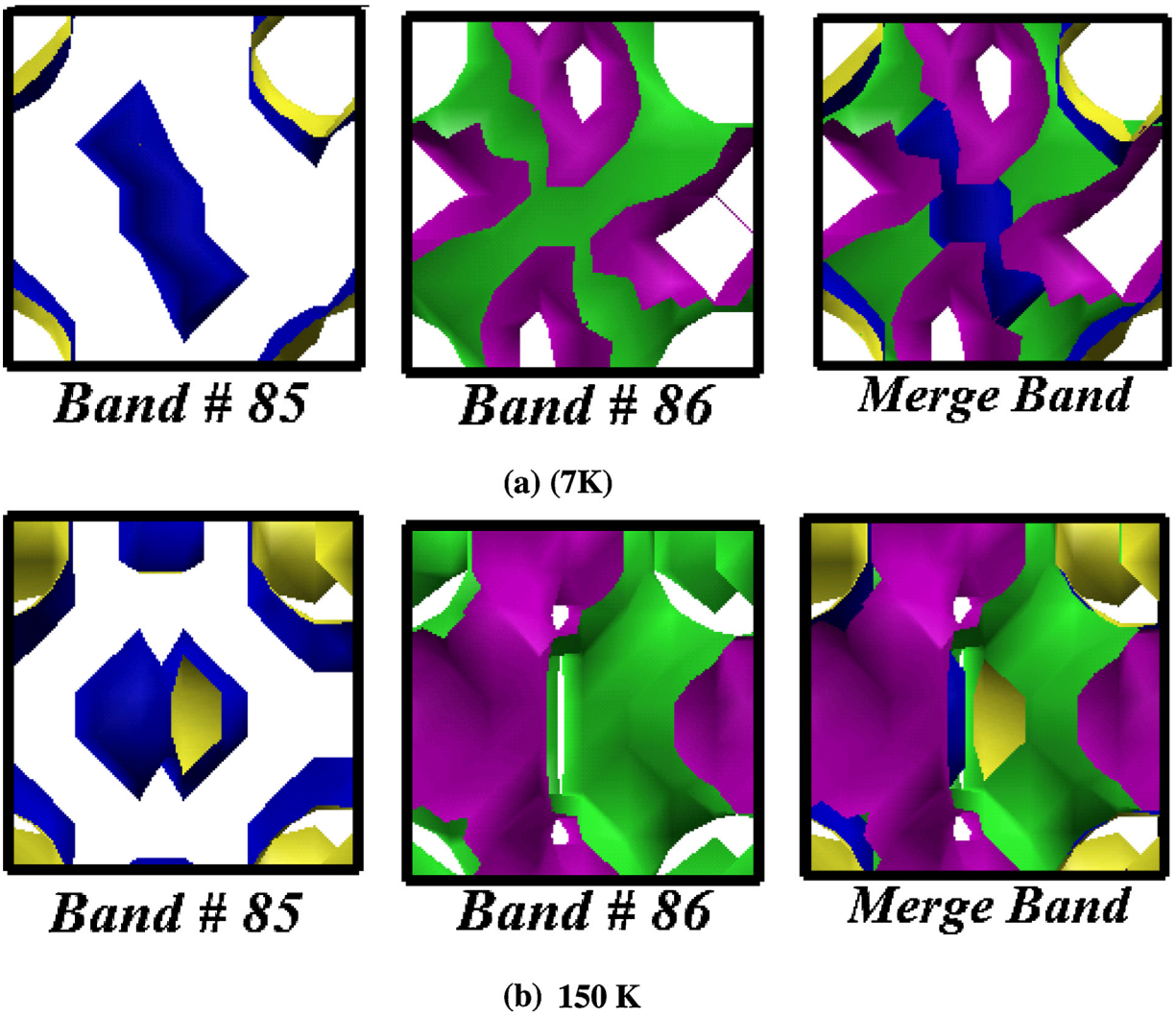

Fig. 5. Calculated Fermi surface of both compounds BPRO (a) 150 K, (b) 7 K.

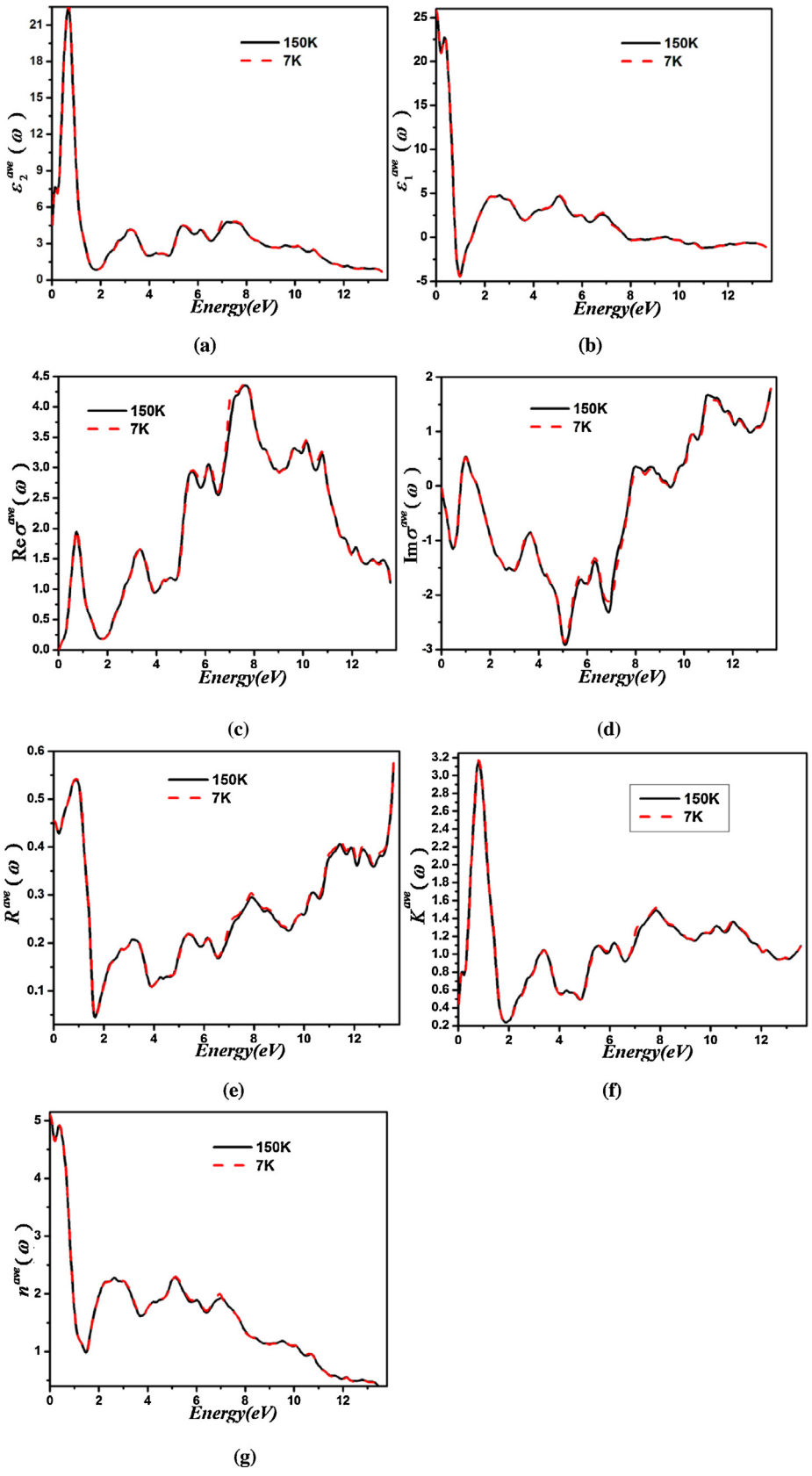

Fig. 6. Calculated average real and imaginary parts of dielectric functions, reflectivity, refractive index, extension coefficients and optical conductivity, of both compounds BPRO (150 K, 7 K) using EVGGA.

momentum matrix elements between the valence and the conduction bands. The Kramers–Kroning transformation [45] is used to obtain the real part $\varepsilon_1(\omega)$ of the dielectric tensor.

We have calculated the average value of frequency dependence real $\varepsilon_1(\omega)$ and imaginary $\varepsilon_2(\omega)$ parts of dielectric function for BPRO compound at 7 K and 150 K as shown in Fig. 6a and b. Due to the metallic nature of the investigated compound we take into account the contribution of the intra-band transitions:

$$\varepsilon(\omega) = \varepsilon_{\text{inter band}}(\omega) + \varepsilon_{\text{intra band}} \quad (3)$$

Fig. 6a shows the average value for the frequency dependence imaginary part $\varepsilon_2{}^{ave}(\omega)$ of the electronic dielectric function for the radiation up to 13.8 eV. In general the dispersion of $\varepsilon_2{}^{ave}(\omega)$ for BPRO (7 K) and BPRO (150 K) is similar. The main peak of $\varepsilon_2{}^{ave}(\omega)$ is situated at around 0.8 eV. At the energies greater than 2.0 eV, several spectral structures were distributed along the energy range.

From the investigation of the optical spectra of $\varepsilon_2{}^{ave}(\omega)$, we notice that the transitions from the bands just below and above the Fermi level are responsible for the spectral structure below 5.0 eV, while the transitions from the bottom of the occupied states to the unoccupied states are responsible for the spectral structure above 5.0 eV.

Fig. 6b shows the average value of the real part $\varepsilon_1{}^{ave}(\omega)$ for BPRO (7 K and 150 K). The sharp rise at low energies is due to the metallic nature of the investigated compounds. The main peak of $\varepsilon_1{}^{ave}(\omega)$ is located at around 0.5 eV.

We also have calculated average value of reflectivity $R^{ave}(\omega)$, optical conductivity $\sigma^{ave}(\omega)$, refractive index $n^{ave}(\omega)$ and extension coefficient $k^{ave}(\omega)$. Fig. 6c and d shows the average value of the real Re $\sigma^{ave}(\omega)$and imaginary Im $\sigma^{ave}(\omega)$ parts of the optical conductivity of both compounds.

It is well known that in the conductivity tensor components, at low energy the intra-band transition play an important role. They are normally represented by Drude formula, which is based on free-electron model:

$$\sigma_D(\omega) = \frac{\omega_P^2}{4\pi(\gamma} D - 1_\omega{}^\gamma) \quad (4)$$

where γ_D = the invers relaxation time and ω_p = the plasma frequency.

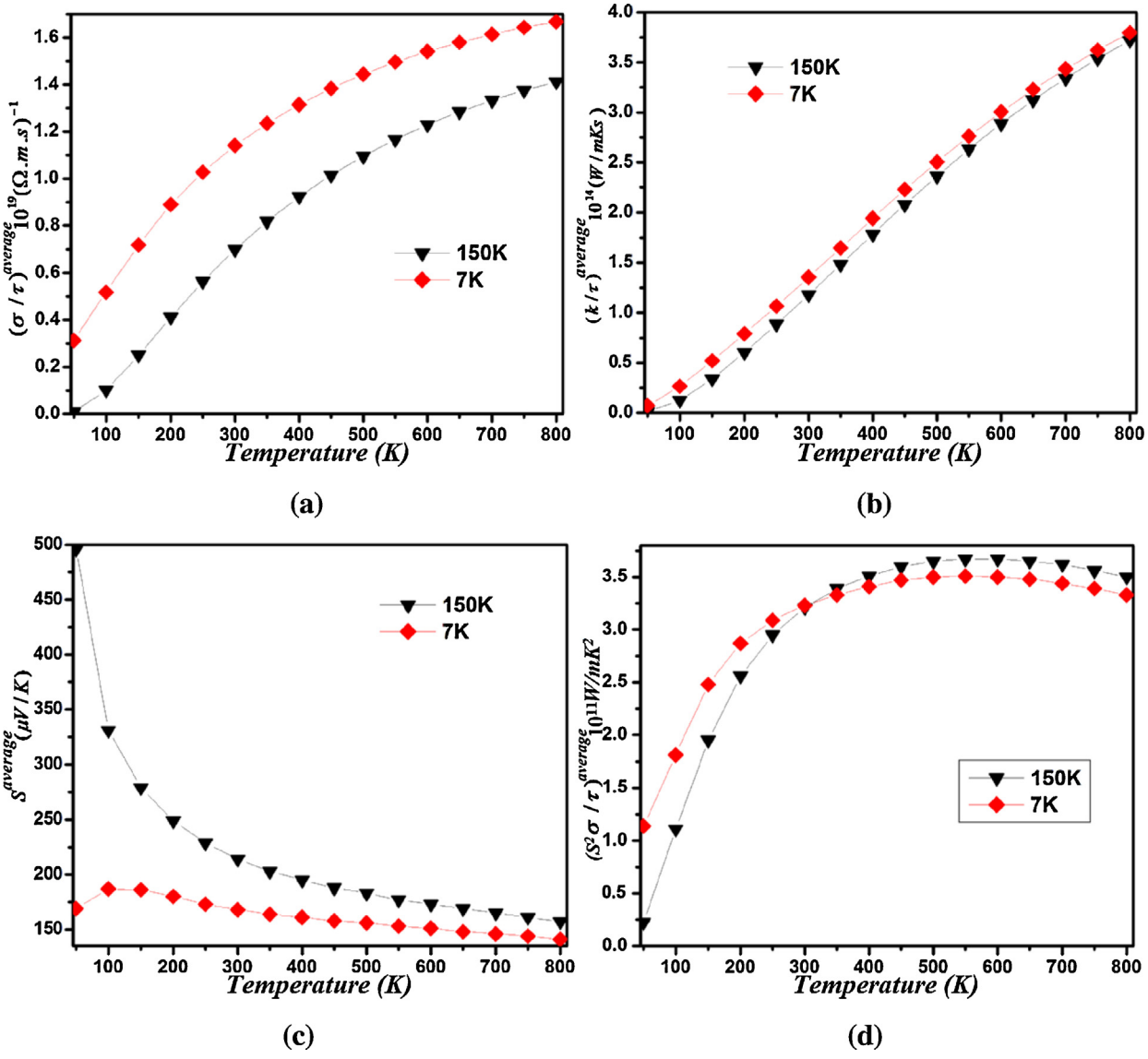

Fig. 7. Calculated transport coefficients of both compounds BPRO (150 K, 7 K) as a function of temperature: electrical conductivity, Seeback coefficient, thermal conductivity and power factor.

In free electron model the relation for the plasma frequency is given by:

$$\omega_P^2 = \frac{4\pi Ne^2}{m} \quad (5)$$

where N = the number of electrons/unit volume.

Generally the spectral peaks in the optical response are determined by the electric–dipole transitions between the occupied and unoccupied bands. The calculated average value of the reflectivity spectra $R^{ave}(\omega)$for BPRO (7 K and 150 K) as a function of energy is shown in Fig. 6e. One can observe that $R^{ave}(\omega)$ spectrum display an abrupt decrease around 1.8 eV which confirm the occurrence of a collective plasmon resonance.

The extension coefficient play very significant role in metals. It shows absorption of energy on the skin of the material. The average value of extension coefficient $k^{ave}(\omega)$ illustrated in Fig. 6f. It is clear that $k^{ave}(\omega)$ is similar for both compounds with minor difference due to the different temperatures (7 K and 150 K). Fig. 6 g, presents the average value of refractive index $n^{ave}(\omega)$ for both compounds. It shows a sharp rise at low energies which confirms the metallic nature of the investigated compounds.

4. Thermoelectric properties

Fig. 7a shows the temperature dependence average electrical conductivity of BPRO (7 k and 150 K). The electrical conductivity is expressed by the following equations within Boltzmann's transport theory

$$\sigma(T, E_F) = \frac{e}{4\pi^3}\int \vec{v}\tau.N(E)\left(-\frac{\partial f}{\partial E}\right)dE \quad (6)$$

where $\vec{v}$ stands for the velocity of the electrons and τ is the relaxation time.

The average value of electrical conductivity of BPRO (150 K) have zero value at 50 K, while BPRO (7 K) shows $0.3 \times 10^{19}(\Omega\,\mathrm{m.s})^{-1}$ at the same temperature. There is an exponential increase in the average value of electrical conductivity due to the increase in temperature to reach its maximum value at 800 K (Fig. 7a). One can see that the coefficient of electrical conductivity show the same behavior in the temperature range from 100 K to 800 K for both compounds, which indicate the superconducting nature of the material.

The average thermal conductivity $k^{ave}(T)$ as a function of temperature for both compounds is shown in Fig. 7b, which show linear increases with increasing the temperature from 50 K to 800 K. It should be emphasize that in the Pr containing thermoelectric materials principle role begin to play electron–phonon anharmonic interactions [46], and one of the specific features of the Pr^{3+} doped oxides is the occurrence of the electron–phonon interactions which change the electron–phonon interaction anharmonicity [47]. In order to explain the phenomenon of scattering, the total thermal conductivity $k_{total}(T)$ is divided into electronic (k_e) as well as lattice (k_{ph}) contributions (usually in BoltzTraP code only the electronic part can be calculated). Above critical temperature, thermal conductivity which depends on temperature follows a T^3 variation in pure superconductor and in the strong scattering technique [48]. It should also be emphasize that for the thermoelectricity principal role is played by electron–phonon contributions [49]. From the plot we observed that thermal conductivity exhibit linear temperature due to weak scattering over greater value of temperature range. At room temperature the thermal conductivity $k^{ave}(T)$ for BPRO (150 K) and BPRO (7 K) is approximately zero and then reaches the maximum value of about 3.7×10^{14} W/mks at 800 K.

We would like to mention here that the transport properties were calculated with constant relaxation time τ. Fig. 7c, shows the average value of Seebeck coefficient $S^{ave}(T)$ vs temperature T within the "random-phase approximation". These $S^{ave}(T)$ of BPRO (150 K) indicates maximum value of about 500 μV/K at 50 K, while BPRO (7 K) depicts lower value of about160 μV/K at 50 K. One can see that BPRO (150 K) shows sharp decraese in $S^{ave}(T)$ at 100 K, whereas BPRO (7 K) show increases in $S^{ave}(T)$ at the same temperature (Fig. 7c). The value of $S^{ave}(T)$ of both compounds decreases exponentially with temperature beyond 150 K. At higher temperature (800 K), BPRO (7 K) show smaller value (145 μV/K) in comparison to BPRO (150 K) 160 μV/K . Which confirm that the investigated compounds show potential applications towards thermoelectric power. This arise come from the fact that the defects and disorder create changes in the electronic properties of the material near the band gape.

In additional we have calculated the average value of Power factor $(S^2\sigma/\tau)^{average}$ vs temperature ranging from 50 K to 800 K for both compounds BPRO (7 K and 150 K) as shown in Fig. 7d. It is clear that $(S^2\sigma/\tau)^{average}$ has different value for both compounds at 50 K i.e., BPRO (7 K) start from1.1×10^{11}W/mK^2 and BPRO (150 K) start from 0.12×1011W/mK2 $(S^2\sigma/\tau)^{average}$ increases exponentially in both compounds, due to the increase of temperature up to 500 K and then start decrease at higher temperature. The maximum value of $(S^2\sigma/\tau)^{average}$ is about 3.7×10^{10}W/mK^2 for BPRO (150 K) and 3.5×10^{10}W/mK^2 for BPRO (7 K) at 150 K. Therefore, both compounds are promising candidates for thermoelectric application, especially BPRO (150 K), because it indicates better thermopower as compared to other one.

5. Conclusions

Here in this work, we have used the first principles calculation to study the electronic structure, optical properties and thermoelectric properties of Ba_2PrRuO_6 single crystals at two different temperatures (7 K and 150 K). From the calculated PDOS, we found that Ba-s, Ru-s, and Pr-s orbital shows strong hybridization in the valance band. It is clear from the band structures that Ru-d and O-p states signify strong contributions around the Fermi level as compared to other states. The calculated results exhibit that the contributions from the states of BPRO (150 K) to the density of states are greater than that of BPRO (7 K). Our investigated compounds depict the superconducting behavior, the values of N (E_F) are 11.5, 12.6, and 16.9 states/eV for BPRO (7 K) and 11.26, 12.02, and 17.6 states/eV for BPRO (150 K). The bare electronic specific heat coefficient is 1.95 (), 2.085 (), and 3.05 () mJ/mol – k^2 for BPRO (150 K), while it is 1.99 (), 2.18 (), and 2.93 () mJ/mol – k^2 for BPRO (7 K). From the study of electronic charge density, it is clear that O atom shows strong sharing with Ru atom than Pr atom and also the ionic nature has been observed between O and Ba atoms. Our investigated Fermi surface shows that BPRO (150 K) have the capability of the good electron transport properties than BPRO (7 K). We also have calculated the optical properties like real and imaginary part of the dielectric function, reflectivity, refractive index, extension coefficient and optical conductivity, in which both intra/inter-band transitions take place. The calculated thermoelectric properties of both compounds show small values of Seebeck coefficient, and higher values of thermal conductivity as well as power factor, which show an increasing behavior with temperature ranging from 50 K to 600 K and suggesting that the compounds indicate potential application for thermoelectric performance at 600 K.

Acknowledgements

This result was developed within the CENTEM project, reg. no. CZ.1.05/2.1.00/03.0088, co-funded by the ERDF as part of the Ministry of Education, Youth and Sports OP RDI program.

MetaCentrum and the CERIT-SC under the program Centre CERIT Scientific Cloud, reg. no. CZ.1.05/3.2.00/08.0144.

References

[1] D. Kirllov, Y. Suzuki, L. Antognazza, K. Char, I. Bozovic, T.H. Geballe, Phys. Rev. B 51 (1995) 12825.
[2] P.D. Battle, C.W. Jones, F. Studer, J. Solid State Chem. 90 (1991) 301.
[3] P.D. Battle, C.P. Gey, M. Hervieu, C. Martin, C.A. Moore, Y. Paik, J. Solid State Chem. 175 (2003) 20.
[4] Y. Doi, Y. Hinatsu, A. Nakamura, Y. Ishii, Y. Morii, J. Mater Chem. 13 (2003) 1758.
[5] N.G. Parkinson, P.D. Hatton, J.A.K. Howard, J. Mater. Chem. 13 (2003) 1468.
[6] R.H. Mitchell, Perovskites Modern and Ancient, Almaz Press Inc, Ontario, 2002.
[7] V.V. Kharton, F.M.B. Marques, A. Atkinson, Solid State Ionics 174 (2004) 135–149.
[8] J.B. Goodenough, Rep. Prog. Phys. 67 (2004) 1915–1993.
[9] S.J. Skinner, Int. J. Inorg. Mater. 3 (2001) 113–121.
[10] T. Ishihara, H. Matsuda, Y. Takita, J. Am. Chem. Soc. 116 (1994) 3801–3803.
[11] N. Bonanos, K.S. Knight, B. Ellis, Solid State Ionics 79 (1995) 161–170.
[12] P. Murugaraj, K.D. Kreuer, T. He, T. Schober, J. Maier, Solid State Ionics 98 (1997) 1–6.
[13] (a) K.D. Kreuer, Solid State Ionics 97 (1997) 1–15;
pt,1>(b) V.V. Kharton, F.M.B. Marques, A. Atkinson, Solid State Ionics 174 (2004) 135–149.
[14] D.C. Ling, S.R. Sheen, C.Y. Tai, J.L. Tseng, M.K. Wu, T.Y. Chen, F.Z. Chien, Proceedings of Xth Anniversary HTS Workshop on Physics Proceedings of Xth Anniversary HTS Workshop on Physics, Materials and Applications, World Scientific, Singapore,, in: B. Batlogg, C.W. Chu, W.K. Chu, D.U. Gubser, K.A. Müller (Eds.), Materials and Applications, World Scientific, Singapore, 1996, pp. 129.
[15] M.K. Wu, D.Y. Chen, F.Z. Chien, S.R. Sheen, D.C. Ling, C.Y. Tai, G.Y. Tseng, D.H. Chen, F.C. Zhang, Z. Phys. B 102 (1997) 37.
[16] D.Y. Chen, F.Z. Chien, D.C. Ling, J.L. Tseng, S.R. Sheen, M.J. Wang, M.K. Wu, Physica C 73 (1997) 282–287.
[17] C. Bernhard, J.L. Tallon, Ch. Niedermayer, Th. Blasius, A. Golnik, E. Brücher, R.K. Kremer, D.R. Noakes, C.E. Stronach, E.J. Ansaldo, Phys. Rev. B 59 (1999) 14099.
[18] C.A. Cardoso, F.M. Araujo-Moreira, V.P.S. Awana, E. Takayama-Muromachi, O.F. de Lima, H. Yamauchi, M. Karppinen, Phys. Rev. B 67 (2003) 020407.
[19] J.W. Lynn, B. Keimer, C. Ulrich, C. Bernhard, J.L. Tallon, Phys. Rev. B 61 (2000) 14964.
[20] R.S. Liu, L.Y. Jang, H.H. Hung, J.L. Tallon, Phys. Rev. B 63 (2001) 212507.
[21] K. Kumagai, S. Takada, Y. Furukawa, Phys. Rev. B 63 (2001) 180509(R).
[22] Y. Maeno, H. Hashimoto, K. Yoshida, S. Nishizaki, T. Fujita, J.G. Bednorz, F. Lichtenberg, Nature 372 (1994) 532.
[23] Y. Izumiyama, Y. Doi, M. Wakeshima, Y. Hinatsu, Y. Shimojo, Y. Morli, J. Phys.: Condens. Matter. 13 (2001) 1303.
[24] Y. Doi, Y. Hinatsu, J. Phys.: Condens. Matter. 11 (1999) 4813.
[25] L. Bauernfeind, W. Widder, H.F. Braun, Physica C 254 (1995) 151.
[26] M.T. Anderson, K.B. Greenwood, G.A. Taylor, K.R. Poeppelmeier, Prog. Solid State Chem. 22 (1993) 197.
[27] P.D. Battle, W.J. Macklin, J. Solid State Chem. 54 (1984) 245.
[28] P.D. Battle, C.W. Jones, J. Solid State Chem. 78 (1989) 108.
[29] Y. Izumiyama, Y. Doi, M. Wakeshima, Y. Hinatsu, Y. Shimojo, Y. Morli, J. Phys.: Condens. Matter. 13 (2001) 1303.
[30] M.K. Wu, D.Y. Chen, F.Z. Chien, S.R. Sheen, D.C. Ling, C.Y. Tai, G.Y. Tseng, D.H. Chen, F.C. Zhang, Z. Phys. B 102 (1997) 37.
[31] D.Y. Chen, F.Z. Chien, D.C. Ling, J.L. Tseng, S.R. Sheen, M.J. Wang, M.K. Wu, Physica C 73 (1997) 282–287.
[32] S.E. Lofland, Mater. Res. Bull. 44 (2009) 1559–1564.
[33] Y. Izumiyama, J. Phys.: Condens. Matter. 13 (2001) 1303–1313.
[34] P. Hohenberg, W. Kohn, Phy. Rev. B 136 (1964) B864.
[35] P. Blaha, K. Schwartz et al. WEIN2K, an augmented plane wave +local orbitals program for calculating crystal properties, Karlheinz Schewarz, Techn, Universita, Wein, Austria, 2001.
[36] W. Kohn, L.J. Sham, Phys. Rev. A 140 (1965) 1133.
[37] F. Zerarga, Solid State Sci. 13 (2011) 1638.
[38] J.P. Perdew, K. Burke, M. Ernzerhof, Phys. Rev. Lett. 77 (1996) 3865.
[39] H.J. Monkhorst, J.D. Pack, Phys. Rev. B 13 (1976) 5188.
[40] A. Rochefort, J. Phys. Chem. B 103 (1999) 641–646.
[41] Y. Izumiyama, J. Phys.: Condens. Matter. 13 (2001) 1303–1313.
[42] P. Vajeeston, P. Ravindran, C. Ravi1, R. Asokamani, Phys. Rev. B 63 (2001) 045115.
[43] A.H. Reshak, S. Azam, J. Magn. Magn. Mater. 342 (2013) 80–86.
[44] A.H. Reshak, Sikander Azam, Int. J. Electrochem. Sci. 8 (2013) 10396–10423.
[45] F.J. Blatt, Physics of electronic conduction in solids, New York: McGraw-Hill (1968) 210.
[46] K. Nouneh, I.V. Kityk, R. Viennois, S. Benet, K.J. Plucinski, S. Charar, Z. Golacki, S. CPaschen, J. Phys. D: Appl. Phys. 38 (2005) 965–973.
[47] A. Brenier, J. Appl. Phys. 90 (2001) 232–236.
[48] M.J. Graf, S.-K. Yip, J.A. Saul, Condensed-Matter 8 (1995) 9509046.
[49] K. Nouneh, Mater. Lett. 61 (2007) 1142–1145.